

Is shrub expansion into grasslands pushed or pulled?

A spatial integral projection model for woody plant encroachment

Trevor Drees^a, Brad M. Ochocki^b, Scott L. Collins^c, and Tom E.X. Miller^{*b}

^aDepartment of Biology, Penn State University, State College, PA USA

^bProgram in Ecology and Evolutionary Biology, Department of BioSciences, Rice University, Houston, TX USA

^cDepartment of Biology, University of New Mexico, Albuquerque, NM USA

October 5, 2022

* Corresponding author: tom.miller@rice.edu

Submitted to *Ecological Monographs*

Manuscript type: Article

Open Research statement: All of our data and code are available during peer review at <https://github.com/TrevorHD/LTEncroachment>. This manuscript and its contents can be reproduced from this file: https://github.com/TrevorHD/LTEncroachment/blob/master/Manuscript/creosote_SIPM_EcologicalMonographs_submission1.Rnw. Upon acceptance, all data will be provided via creation and publication of an Environmental Data Initiative (EDI) data package, and code will be archived via Zenodo.

Abstract

The encroachment of woody plants into grasslands is a global phenomenon with implications for biodiversity and ecosystem function. Understanding and predicting the pace of expansion and the underlying processes that control it are key challenges in the study and management of woody encroachment. Theory from spatial population biology predicts that the occurrence and speed of population expansion should depend sensitively on the nature of conspecific density dependence. If fitness is maximized at the low-density encroachment edge then shrub expansion should be “pulled” forward. However, encroaching shrubs have been shown to exhibit positive feedbacks, whereby shrub establishment modifies the environment in ways that facilitate further shrub recruitment and survival. In this case there may be a fitness cost to shrubs at low density causing expansion to be “pushed” from behind the leading edge. We studied the spatial dynamics of creosotebush (*Larrea tridentata*), which has a history of encroachment into Chihuahuan Desert grasslands over the past century. We used observational data and seedling transplant experiments to test the strength and direction of density dependence in shrub demographic performance along a gradient of shrub density at the grass-shrub ecotone. We also used seed-drop experiments and wind data to construct a mechanistic seed dispersal kernel, then connected demography and dispersal data within a spatial integral projection model (SIPM) to predict the dynamics of shrub expansion. The SIPM predicted that, contrary to expectations based on potential for positive feedbacks, the shrub encroachment wave is “pulled” by maximum fitness at the low-density front. However, the predicted pace of expansion was strikingly slow (ca. 8 cm/yr), and this prediction was supported by independent re-surveys of the ecotone showing little to no change in spatial extent of shrub cover over 12 years. Encroachment speed was

25 acutely sensitive to seedling recruitment, suggesting that this population may be primed
26 for pulses of expansion under conditions that are favorable for recruitment. Our inte-
27 gration of observations, experiments, and modeling reveals not only that this ecotone is
28 effectively stalled under current conditions, but also *why* that is so and how that may
29 change as the environment changes.

30 **Keywords**

31 density-dependence, ecotones, woody encroachment, shrubs, integral projection model,
32 dispersal, Allee effects

Introduction

The recent and ongoing encroachment of shrubs and other woody plants into adjacent grasslands has caused significant vegetation changes across arid and semi-arid landscapes worldwide (Cabral et al., 2003; Gibbens et al., 2005; Goslee et al., 2003; Parizek et al., 2002; Roques et al., 2001; Trollope et al., 1989; Van Auken, 2009, 2000). The process of encroachment generally involves increases in the number or density of woody plants in both time and space (Van Auken, 2000), which can drive shifts in plant community structure and alter ecosystem processes (Knapp et al., 2008; Ravi et al., 2009; Schlesinger and Pilmanis, 1998; Schlesinger et al., 1990). Other effects of encroachment include changes in ecosystem services (Kelleway et al., 2017; Reed et al., 2015), declines in biodiversity (Brandt et al., 2013; Ratajczak et al., 2012; Sirami and Monadjem, 2012), and economic losses in areas where the proliferation of shrubs adversely affects grazing land and pastoral production (Mugasi et al., 2000; Oba et al., 2000).

Woody plant encroachment can be studied through the lens of spatial population biology as a wave of individuals that may expand across space and over time (Kot et al., 1996; Neubert and Caswell, 2000; Pan and Lin, 2012; Wang et al., 2002). Theory predicts that the speed of wave expansion depends on two processes: local demography and dispersal of propagules. First, local demographic processes include recruitment, survival, growth, and reproduction, which collectively determine the rate at which newly colonized locations increase in density and produce new propagules. Second, colonization events are driven by the spatial dispersal of propagules, which is commonly summarized as a probability distribution of dispersal distances, or “dispersal kernel”. The speed at which expansion waves move is highly dependent upon the shape of the dispersal kernel and can be strongly influenced by long-distance dispersal events in the tail of the

57 distribution (Skarpaas and Shea, 2007). Both demography and dispersal may depend
58 on plant size, since larger plants often have improved demographic performance and
59 release seeds from greater heights, leading to longer dispersal distances (Nathan et al.,
60 2011). Accounting for population structure, including size structure, may therefore be
61 important for understanding and predicting wave expansion dynamics (Neubert and
62 Caswell, 2000).

63 Theory predicts that the nature of conspecific density dependence is another critical
64 feature of expansion dynamics but this is rarely studied in the context of woody plant
65 encroachment. Expansion waves typically correspond to gradients of conspecific den-
66 sity – high in the back and low at the front – and demographic rates may be sensitive
67 to density due to intraspecific interactions like competition or facilitation. If the demo-
68 graphic effects of density are strictly negative due to competitive effects that increase
69 with density, then demographic performance is maximized as density goes to zero at the
70 leading edge of the wave. Under these conditions, the wave is “pulled” forward by in-
71 dividuals at the low-density vanguard (Kot et al., 1996), and targeting these individuals
72 and locations would be the most effective way to slow down or prevent encroachment.
73 However, woody encroachment systems often involve positive feedbacks whereby shrub
74 establishment modifies the environment in ways that facilitate further shrub recruitment.
75 For example, woody plants can modify their micro-climates in ways that elevate night-
76 time minimum temperatures, promoting conspecific recruitment and survival for freeze-
77 sensitive species (D’odorico et al., 2013; Huang et al., 2020). Positive density dependence
78 (or Allee effects) causes demographic rates to be maximized at higher densities behind
79 the leading edge, which “push” the expansion forward, leading to qualitatively different
80 expansion dynamics (Kot et al., 1996; Lewis and Kareiva, 1993; Sullivan et al., 2017; Taylor
81 and Hastings, 2005; Veit and Lewis, 1996). Pushed expansion waves generally have dif-

ferent shapes (steeper density gradients) and slower speeds than pulled waves (Gandhi et al., 2016), and may require different strategies for managing or decelerating expansion (Taylor and Hastings, 2005). Under some conditions, positive density dependence can cause expansion to fail entirely, “pinning” populations in place (Keitt et al., 2001). The potential for positive feedbacks is well documented in woody encroachment systems as a key feature of bi-stability (the existence of woody and herbaceous habitats as alternative stable states: Wilcox et al. (2018)) but it remains unclear whether and how strongly these feedbacks decelerate shrub expansion and influence strategies for management of woody encroachment.

In this study, we linked woody plant encroachment to ecological theory for spreading populations, with the goals of understanding how seed dispersal and density-dependent demography drive encroachment, and determining whether the encroachment wave is pushed or pulled. Throughout the aridlands of the southwestern United States, shrub encroachment into grasslands is well documented (D’Odorico et al., 2012) but little is known about the dispersal and demographic processes that govern it. Our work focused on creosotebush (*Larrea tridentata*) in the northern Chihuahuan Desert. This native shrub has encroached into grasslands over the past 150 years, leading to decreased cover of black grama grass (*Bouteloua eriopoda*), the dominant foundation species of Chihuahuan desert grassland (Buffington and Herbel, 1965; Gardner, 1951; Gibbens et al., 2005). As in many woody encroachment systems, creosotebush expansion generates ecotones marking a transition from dense shrubland to open grassland, with a transition zone in between where shrubs can often be found interspersed among grasses (Fig. 1).

Historically, creosotebush encroachment into grasslands is believed to have been driven by a combination of factors including overgrazing, drought, variability in rainfall, and suppression of fire regimes (Moreno-de las Heras et al., 2016). These shrubs

are also thought to further facilitate their own encroachment through positive feedbacks (D’Odorico et al., 2012; Grover and Musick, 1990) by modifying their environment in ways that favor continued growth and recruitment, including changes to the local microclimate (D’Odorico et al., 2010) and rates of soil erosion (Turnbull et al., 2010). Such positive feedbacks also involve suppression of herbaceous competitors, reducing competition as well as the amount of flammable biomass used to fuel the fires that keep creosotebush growth in check (Van Auken, 2000). We hypothesized that, given potential for positive feedback mechanisms, the rarity of conspecifics at the low-density encroachment front may depress demographic performance and generate pushed-wave dynamics.

We used a combination of observational and experimental data from shrub ecotones in central New Mexico to parameterize a spatial integral projection model (SIPM) that predicts the speed of encroachment (m/yr) resulting from lower-level demographic and dispersal processes. Our data came from demographic surveys and experimental transplants along replicate ecotone transects spanning a gradient of shrub density, and from seed drop experiments to estimate the properties of the dispersal kernel. We focused on wind dispersal of seeds, since little is known about the natural history of dispersal in this system and the seeds lack adaptations to attract frugivorous animals, such as bright coloration or fleshy fruit, though they may be moved by granivores. Given the challenges of directly measuring seed dispersal, we instead built mechanistic dispersal kernels that predict seed movement based on properties of maternal plants, seeds, and wind; because it does not account for secondary biotic or abiotic dispersal vectors, this approach provided a conservative first step toward understanding seed movement. We also used re-surveys of permanent transects as an independent measure of encroachment that provided a benchmark against which to evaluate model predictions. The SIPM accounts for size-structured demography of creosotebush, allows us to test whether shrub expansion

132 is pulled by the low-density front or pushed from the high-density core, and identi-
133 fies the local (demographic) and spatial (seed dispersal) life cycle transitions that most
134 strongly contribute to expansion speed. We address the following specific questions:

- 135 1. What are the strength and direction of density dependence in demographic vital
136 rates along shrub encroachment ecotones?
- 137 2. What is the seed dispersal kernel and how does it vary with maternal plant size?
- 138 3. What is the predicted rate of expansion and which lower-level processes most
139 strongly affect the expansion speed?
- 140 4. How does the observed rate of encroachment in the recent past compare to model
141 predictions?

142 **Materials and methods**

143 *Study species*

144 Creosotebush (*Larrea tridentata*) is a perennial, drought-resistant shrub that is native to
145 the arid and semiarid regions of the southwestern United States and northern Mexico.
146 High-density areas of creosotebush consist largely of barren soil between plants due to
147 the “islands of fertility” these shrubs create around themselves (Reynolds et al., 1999;
148 Schlesinger et al., 1996), though lower-density areas will often contain grasses in the
149 inter-shrub spaces (Fig. 1). Elsewhere in North America creosotebush can produce clonal
150 rings though asexual reproduction (Vasek, 1980) but this does not occur in our northern
151 Chihuahuan desert study region, where creosotebush genetic diversity is high (Duran
152 et al., 2005). The small yellow flowers of creosotebush give rise to pubescent spherical
153 fruits several *mm* in diameter; these fruits consist of five carpels, each of which contains

154 a single seed. Seeds are dispersed from the parent plant by gravity and wind, with the
155 possibility for seeds to subsequently be transported by animals or water (Maddox and
156 Carlquist, 1985). The foliage is dark green, resinous, and unpalatable to most grazing
157 and browsing animals (Mabry et al., 1978).

158 *Study site*

159 We conducted our work at the Sevilleta National Wildlife Refuge (SNWR), a Long-Term
160 Ecological Research (SEV-LTER) site in central New Mexico. The refuge exists at the in-
161 tersection of several eco-regions, including the northern Chihuahuan Desert, Great Plains
162 grassland, and steppes of the Colorado Plateau. Annual precipitation is approximately
163 250mm, with the majority falling during the summer monsoon from June to September.
164 The recruitment events that facilitate creosotebush expansion are thought to be episodic
165 (Peters and Yao, 2012), and this may be linked to fluctuations in monsoon precipitation
166 (Bowers et al., 2004; Boyd and Brum, 1983).

167 *Demographic data*

168 *Ecotone transects*

169 We collected demographic data during early June of every year from 2013-2017. This
170 work was conducted at four sites in the eastern part of SNWR (one site was initiated in
171 2013 and the other three in 2014), with three transects at each site. All transects were
172 situated along a shrubland-grassland ecotone so that a full range of shrub densities was
173 captured: each transect spanned core shrub areas, grassland with no or few shrubs,
174 and the transition between them. Lengths of these transects varied from 200 to 600 m
175 and were determined by the strength of vegetation transition since “steep” transitions

176 required less length to capture the full range of shrub density.

177 We quantified shrub density in 5-meter “windows” along each transect, including all
178 shrubs within one meter of the transect on either side (shrubs that partially overlapped
179 with the census area were included). Densities were quantified once for each transect
180 (in 2013 or 2014) and were assumed to remain constant for the duration of the study, a
181 reasonable assumption for a species with very low recruitment and very high survival of
182 established plants (see Results). Given the population’s size structure, we weighted the
183 density of each window by the sizes of the plants, which we quantified as volume (cm^3).
184 Volume was calculated as that of an elliptic cone (McAuliffe et al., 2007): $V_i = \frac{\pi h}{3} \frac{lw}{4}$
185 where l , w , and h are the maximum length, maximum width, and height, respectively.
186 Maximum length and width were measured so that they were always perpendicular to
187 each other, and height was measured from the base of the woody stem at the soil surface
188 to the tallest part of the shrub. The weighted density for a window was then expressed
189 as $\log(\text{volume})$ summed over all plants in the window.

190 *Observational census*

191 At approximately 50-m intervals along each transect we tagged up to 10 plants for annual
192 demographic census and recorded their local (5-m resolution) window so that we could
193 connect individual demographic performance to local density. These tagged shrubs were
194 revisited every June and censused for survival (alive/dead), size (width, length, and
195 height, as above), flowering status, and fertility of flowering plants (numbers of flower-
196 buds, flowers, and fruits). In instances where shrubs had large numbers of reproductive
197 structures that would be difficult to reliably count (a large shrub may have thousands of
198 flowers or fruits), we made counts on a fraction of the shrub and extrapolated to esti-
199 mate whole-plant reproduction. Creosotebush does not have one discrete reproductive

200 event per year; instead, flowering may occur throughout much of the warm season. By
201 combining counts of buds, flowers, and fruits we intended to capture a majority of the
202 season's reproductive output, assuming that all buds and flowers will eventually become
203 fruits. Our measurements of reproductive output are therefore conservative and may un-
204 derestimate total seed production for an entire transition year. Each year, we searched
205 for new recruits within 1m on either side of the transect. New recruits were tagged
206 and added to the demographic census. The observational census included a total of 522
207 unique individuals.

208 *Transplant experiment*

209 We conducted a transplant experiment in 2015 to test how shrub density affects seedling
210 survival. This approach complemented observational estimates of density dependence
211 and filled in gaps for a part of the shrub life cycle that was rarely observed due to low
212 recruitment. Seeds for the experiment were collected from plants in our study popu-
213 lation in 2014. Seeds were germinated on Pro-Mix potting soil (Quakertown, PA) in
214 Fall 2014 and seedlings were transferred to 3.8 cm-by-12.7 cm cylindrical containers and
215 maintained in a greenhouse at Rice University. Seedlings were transported to SNWR
216 and transplanted into the experiment during July 27-31, 2015. Transplant timing was
217 intended to coincide with the monsoon season, when most natural recruitment occurs.

218 The transplant experiment was conducted at the same four sites and three transects
219 per site as the observational demographic census, where we knew weighted shrub den-
220 sities at 5-m window resolution. We established 12 1-m by 1-m plots along each transect
221 and these were intentionally placed to capture density variation: four plots were in win-
222 dows with zero shrubs, four plots were placed in the top four highest-density windows
223 on the transect, and the remaining four plots were randomly distributed among the re-

224 maining windows with weighted density greater than zero. Plots were placed in the
225 middle of each 5-m window (at meter 2.5) and were divided into four 0.5-m by 0.5-m
226 subplots. We divided each subplot into nine squares (0.125-m by 0.125-m) and recorded
227 ground cover of each square as one of the following categories: bare ground, creosote-
228 bush, black grama (*B. eriopoda*), blue grama (*B. gracilis*), other grass, or “other”. Each
229 subplot received one transplanted shrub seedling, for a total of 48 transplants per tran-
230 sect, 144 transplants per site, and 576 transplants in the entire experiment. Each site was
231 set up on a different day and there was a significant monsoon event between setup of the
232 third and fourth sites. This resulted in differential mortality that appears to be related
233 to site (captured as a statistical random effect) but more likely reflects the timing of the
234 monsoon event relative to planting (moist soil likely promoted transplant survival). We
235 revisited the transplant experiment on October 24, 2015 to survey mortality. After that
236 first visit, transplants were censused along with the naturally occurring plants each June,
237 following the methods described above.

238 *Demographic analysis*

239 We fit statistical models to the demographic data and used AIC-based model selection to
240 evaluate empirical support for alternative candidate models. The top statistical models
241 were then used as the vital rate sub-models of the SIPM, so there is a strong connection
242 between the statistical and population modeling, as is typical of integral projection mod-
243 eling. Our analyses focused on the following demographic vital rates: survival, growth,
244 probability of flowering, fertility (flower and fruit production), seedling recruitment, and
245 seedling size. Most of these vital rates were modeled as a function of plant size, and all
246 of them included the possibility of density dependence.

247 The alternative hypotheses of pushed versus pulled wave expansion rest on how the

248 rate of population increase (λ), derived from the combination of all vital rates, respond
249 to density. We were particularly interested in whether demographic performance was
250 maximized as local density goes to zero (pulled) or at non-zero densities behind the
251 wave front (pushed). To flexibly model density dependence and detect non-monotonic
252 responses, we used generalized additive models in the R package ‘mgcv’ (Wood, 2017).
253 For each vital rate, we fit candidate models with or without a smooth term for local
254 weighted density, among other possible covariates. To avoid over-fitting, we set the
255 ‘gamma’ argument of `gam()` to 1.8, which increases the complexity penalty, results in
256 smoother fits (Wood, 2017), and makes our approach more conservative (other gamma
257 values yielded qualitatively similar results). We pooled data across transition years for
258 analysis. All models included the random effect of transect (12 transects across 4 sites);
259 we did not attempt to model both site and transect-within-site random effects due to the
260 low numbers of each. All vital rate functions used the natural logarithm of volume (cm^3)
261 as the size variable and the sum of $\log(\text{volume})$ as the weighted density of a transect
262 window.

263 *Survival.* We modeled survival or mortality in year $t + 1$ as a Bernoulli random variable
264 with three candidate models for survival probability. These included smooth terms for
265 initial size in year t only (1), initial size and weighted density (2), and both smooth terms
266 plus an interaction between initial size and weighted density (3). We analyzed survival of
267 experimental transplants and observational census plants together in the same analyses,
268 with a fixed effect of transplant status (yes/no) included in all candidate models. Since
269 recruits and thus mortality events were both very rare in the observational survey, this
270 approach allowed us to “borrow strength” over both data sets to generate a predictive
271 function for size- and possibly density-dependent survival while statistically accounting
272 for differences between experimental and naturally occurring plants. Because we had

273 additional, finer-grained cover data for the transplant experiment that we did not have
274 for the observational census, we conducted an additional stand-alone analysis of trans-
275 plant survival that explored the influence of shrub and grass density at multiple spatial
276 scales (Appendix C).

277 *Growth.* We modeled size in year $t + 1$ as a Gaussian random variable, with nine can-
278 didate models for growth. The simplest model (1) defined the mean of size in year $t + 1$
279 as a smooth function of size in year t and constant variance. Models (2) and (3) had con-
280 stant variance but the mean included smooth terms for initial size and weighted density
281 (2) or both smooth terms plus an interaction between initial size and weighted density
282 (3). Models 4-6 had the same mean structure as 1-3 but defined the standard deviation
283 of size in year $t + 1$ as a smooth function of initial size. Models 7-9 mirrored 4-6 and
284 additionally included a smooth term for weighted density in the standard deviation.
285 Modeling growth correctly is important because it defines the probability of any future
286 size conditional on current size, a critical element of the IPM transition kernel. We veri-
287 fied that the AIC-selected model described the data well by simulating data from it and
288 comparing the moments (mean, variance, skewness, and kurtosis) of simulated and real
289 data.

290 *Flowering and fruit production.* We modeled shrub reproductive status (vegetative or
291 flowering) in year t as a Bernoulli random variable with three candidate models for
292 flowering probability. These included smooth terms for current size (in year t) only (1),
293 size and weighted density (3), and both smooth terms plus an interaction between size
294 and weighted density. We modeled the reproductive output of flowering plants (the sum
295 of flowerbuds, open flowers, and fruits) in year t as a negative binomial random variable.
296 There were three candidate models for mean reproductive output that corresponded to

297 the same three candidates for flowering probability.

298 *Recruitment and recruit size.* We modeled seedling recruitment in each transect window
299 as a binomial random variable given the number of total seeds produced in that window
300 in the preceding year. There were two candidate models, with and without an influence
301 of weighted density on the per-seed recruitment probability. To estimate window-level
302 seed production, we used the best-fit models for flowering and fruit production and
303 applied this to all plants in each window that we observed in our initial density surveys.
304 We assume that recruits come from the previous year's seeds and not from a long-lived
305 soil seed bank. This assumption might lead us to over-estimate the recruitment rate, since
306 existence of a seed bank would inflate the denominator of seedlings-per-seed. However,
307 a previous study at SNWR found relatively low densities of viable creosotebush seeds
308 in soil, suggesting that this species does not form a persistent seed bank (Moreno-de las
309 Heras et al., 2016).

310 We modeled recruit size as a Gaussian-distributed random variable and fit four can-
311 didate models including an influence of weighted density on mean, variance, both, and
312 neither.

313 *Density-dependent IPM*

314 The size- and density-dependent statistical models comprised the sub-models of a den-
315 sity dependent Integral Projection Model (IPM) that we used to evaluate how the shrub
316 population growth rate responded to conspecific density; we present this non-spatial
317 model before layering on the spatial dynamics generated by seed dispersal. A basic
318 density-independent IPM predicts the number of individuals of size x' at time $t + 1$
319 ($n(x', t + 1)$) based on a demographic projection kernel (K_{dem}) that gives the rates of tran-
320 sition from sizes x to x' from times t to $t + 1$ and is integrated over the size distribution

321 from the minimum (x_{min}) to maximum (x_{max}) sizes. In a density-dependent IPM, com-
 322 ponents of the projection kernel may respond to population abundance and structure:

$$323 \quad n(x', t + 1) = \int_{x_{min}}^{x_{max}} K_{dem}(x', x, \tilde{n}(t)) n(x, t) dx \quad (1)$$

324 Here, $\tilde{n}(t)$ is some function of population structure $n(x, t)$ such as the total density of
 325 conspecifics ($\tilde{n}(t) = \int n(x, t) dx$) or, as in our case, total density weighted by size ($\tilde{n}(t) =$
 326 $\int xn(x, t) dx$). For simplicity, in the analyses that follow we do not model density as
 327 a dynamic state variable; instead, we treat density as a static covariate ($\tilde{n}(t) = \tilde{n}$) and
 328 evaluate the IPM at a range of density values. As in our statistical modeling, the size
 329 variable of the IPM (x, x') was $\log(cm^3)$.

330 For our model, the size- and density-dependent demographic transitions captured by
 331 the projection kernel include growth or shrinkage (g) from size x to x' conditioned on
 332 survival (s) at size x (combined growth-survival function $G(x', x, \tilde{n}) = g(x', x, \tilde{n})s(x, \tilde{n})$),
 333 and the production of new size- x' individuals from size- x parents ($Q(x', x, \tilde{n})$). Repro-
 334 duction reflects the probability of flowering at size x (p), the number of seeds produced
 335 by flowering plants (d), the per-seed probability of recruitment (m), and the size distri-
 336 bution of recruits (c). Collectively, the rate at which x -sized individuals produce x' -sized
 337 individuals at density \tilde{n} is given by the combined reproduction-recruitment function
 338 $Q(x', x, \tilde{n}) = p(x, \tilde{n})d(x, \tilde{n})m(\tilde{n})c(x', \tilde{n})$. Thus, we can express the projection kernel as:

$$339 \quad K_{dem}(x', x, \tilde{n}) = G(x', x, \tilde{n}) + Q(x', x, \tilde{n}) \quad (2)$$

340 For analysis, we evaluated the IPM kernel over a range of local densities from the min-
 341 imum to the maximum of weighted density values observed in the 5-meter windows
 342 ($0 \leq \tilde{n} \leq \tilde{n}_{max}$). At each density level, we discretized the IPM kernel into a 200×200

matrix and calculated the asymptotic growth rate $\lambda(\tilde{n})$ as its leading eigenvalue. We extended the lower (x_{min}) and upper (x_{max}) integration limits to avoid unintentional “eviction” using the floor-and-ceiling method (Williams et al., 2012).

We sought to characterize the shape of density dependence – whether fitness declined monotonically or not with increasing density – and quantified uncertainty in the density-dependent growth rate $\lambda(\tilde{n})$ by bootstrapping our data. For each bootstrap, we randomly sampled 75% of our demographic data, re-ran the statistical modeling and model selection, and used the top vital rate models to generate $\lambda(\tilde{n})$ for that data subset. We repeated this procedure for 500 bootstrap replicates.

Dispersal modelling

WALD dispersal model. Dispersal kernels were calculated using the WALD, or Wald analytical long-distance dispersal, model that uses a mechanistic approach to predict dispersal patterns of plant propagules by wind. The WALD model, which is based in fluid dynamics, can serve as a good approximation of empirically-determined dispersal kernels (Katul et al., 2005; Skarpaas and Shea, 2007) and may be used when direct observations of dispersal are not available. Under the assumptions that wind turbulence is low, wind flow is vertically homogenous, and terminal velocity is achieved immediately upon seed release, the WALD model simplifies a Lagrangian stochastic model to create a dispersal kernel that estimates the likelihood a propagule will travel a given distance (Katul et al., 2005). Our dispersal kernel takes the form of the inverse Gaussian distribution, using r to denote dispersal distance:

$$p(r) = \left(\frac{\lambda'}{2\pi r^3} \right)^{\frac{1}{2}} \exp \left[-\frac{\lambda'(r - \mu')^2}{2\mu'^2 r} \right] \quad (3)$$

Here, λ' is the location parameter and μ' is the scale parameter, which depend on

environmental and plant-specific properties of the study system. (We use λ' for consistency with notation in related papers, but λ' the dispersal location parameter should not be confused with λ the geometric growth rate.) The location and scale parameters are defined as $\lambda' = (H/\sigma)^2$ and $\mu' = HU/F$; these are functions of the height H of seed release, wind speed U at seed release height, seed terminal velocity F , and the turbulent flow parameter σ that depends on both wind speed and local vegetation roughness. We parameterized the WALD dispersal kernel using windspeed data from the SEV-LTER weather station nearest our study site (Moore and Hall, 2022) and seed terminal velocity data from laboratory-based seed-drop experiments (Appendix A). We integrated the dispersal kernel over observed variation in wind speeds, seed terminal velocity, and release height within the height of a shrub. Therefore the dispersal kernel for a shrub of height H was given by:

$$K_{disp} = \iiint p(F)p(U)p(z)p(r) dF dU dz \quad (4)$$

and $p(F)$ and $p(U)$ are the PDFs of the terminal velocity F and wind speed U , respectively, and $p(z)$ is the uniform distribution from the minimum seed release height (0.15m, the height at which grass cover interferes with wind dispersal) to H . Methods for our seed data collection and technical details of dispersal kernel modeling are provided in Appendix A.

Spatial integral projection model

We used a spatial integral projection model to piece together seed dispersal and density-dependent demography, and generate predictions for the rate of shrub expansion that results from this combination of local and spatial processes. The spatially explicit model builds upon the non-spatial model (Eq. 1) and adds a spatial variable (z, z') such that

demographic transitions occur across both time and space according to a combined
 demography-dispersal kernel \tilde{K} :

$$n(x', z', t + 1) = \int_{-\infty}^{+\infty} \int_{x_{min}}^{x_{max}} \tilde{K}(x', x, z', z, \tilde{n}(z, t)) n(x, z, t) dx dz \quad (5)$$

Here, $\tilde{K}(x', x, z', z, \tilde{n}(z, t))$ describes the transition from size x and location z to size x'
 and location z' given density $\tilde{n}(z, t)$ at starting location z . As before, \tilde{n} is a function of
 population structure – in our model, weighted local density – but here integrated over
 an explicit competitive “neighborhood”:

$$\tilde{n}(z, t) = \int_{z-h}^{z+h} \int_{x_{min}}^{x_{max}} x n(x, z, t) dx dz \quad (6)$$

where h represents neighborhood size in the units of z . The demography-dispersal
 kernel \tilde{K} is given by the sum of two parts, one that describes reproduction coupled
 with dispersal of propagules, and another that describes growth and survival of non-
 dispersing individuals:

$$\tilde{K}(x', x, z', z, \tilde{n}(z, t)) = K_{disp}(z' - z)Q(x', x, \tilde{n}) + \delta(z' - z)G(x', x, \tilde{n}) \quad (7)$$

Here, the regeneration function Q and growth-survival function G correspond to Eq.
 2, dispersal kernel K_{disp} corresponds to Eq. 7, and the Dirac delta function ($\delta(z' - z)$) is a
 probability distribution with all mass at zero, which prevents movement during survival
 and size transition. Following standard assumptions for integro-difference equations,
 we assume that space is one-dimensional and homogeneous, such that demographic
 transitions do not depend on location (or, more precisely, that they depend on location
 only through spatial variation in density) and the probability of dispersing from location
 z to z' depends only on the absolute distance between them.

Under many conditions, models of this form generate traveling waves, and we are particularly interested in the velocity (m/yr) of this wave. Methods to estimate this velocity depend strongly on how demography responds to density. If fitness is maximized at some density $\tilde{n} > 0$ then the wave is pushed and wave velocity can only be estimated through numerical simulation. However, if fitness is maximized at $\tilde{n} = 0$ then the wave is pulled and an upper bound on its asymptotic velocity can be calculated analytically, following Neubert and Caswell (2000) and Jongejans et al. (2011), as

$$c^* = \min_{s>0} \left[\frac{1}{s} \ln(\rho_s) \right] \quad (8)$$

where s is a wave shape parameter and ρ_s is the dominant eigenvalue of the kernel $H_s(x', x)$. Corresponding to Eq. 7 and assuming $\tilde{n} = 0$, H_s is composed of

$$H_s(x', x) = M(s, x)Q(x', x) + G(x', x) \quad (9)$$

where $M(s, x)$ is the moment-generating function (MGF) for the dispersal kernel associated with size x . This formulation of the model assumes that the dispersal kernel depends only on maternal size x and not offspring size x' . To estimate $M(s, x)$ we simulated $N = 10000$ dispersal events (r) for each size x and marginalized these over one spatial dimension as in Lewis et al. (2006). We then evaluated the empirical MGF for each size x : $M(s) = \frac{1}{N} \sum_{i=1}^N e^{sr}$.

We used numerical sensitivity analysis to compare the contributions of demography and dispersal processes to the speed of expansion. We perturbed each vital rate function by an arbitrary value, recalculated wavespeed, and quantified sensitivity as the change in wavespeed divided by the perturbation. Analytical sensitivity analysis is also possible (Ellner et al., 2016) but these sensitivities reflect infinitesimally small perturbations. We

432 were particularly interested in the effects of large perturbations, especially large changes
433 in seedling recruitment, which is subject to pulse events.

434 Estimates of wavespeed and its sensitivity to demography and dispersal processes
435 were bootstrapped for a total of 1000 replicates. Each bootstrap replicate recreated size-
436 and density-dependent demographic models using 50% resampling on the original de-
437 mographic data, and recreated dispersal kernels also using 75% resampling on the wind
438 speeds and seed terminal velocities. Model selection for demographic vital rates was re-
439 run for each bootstrap replicate. The empirical MGF relied on numerical sampling and
440 was therefore sensitive to extreme long-distance events that differed across bootstrap
441 realizations. Therefore, bootstrapped distributions reflect the combination of model un-
442 certainty, parameter uncertainty, and stochasticity inherent to empirical MGFs.

443 *Encroachment re-surveys*

444 Finally, we used re-survey data from permanent transects to assess the predictions of
445 the SIPM with respect to independent empirical observations. In summer 2001, shrub
446 percent cover was recorded along two permanent 1000-m transects that spanned the
447 shrub-grass ecotone (these were different transects than those described above for shrub
448 demography). Surveys were conducted again in summer 2013 to document change in cre-
449 osotebush abundance and spatial extent. At every 10 meters, shrub cover was recorded
450 in nine cover classes (<1%, 1–4%, 5–10%, 10–25%, 25–33%, 33–50%, 50–75%, 75–95%,
451 >95%). For visualization, we show midpoint values of these cover classes at each meter
452 location for both transects and years.

Results

What are the strength and direction of density dependence in demographic vital rates along shrub encroachment ecotones?

Demographic data from naturally occurring and transplanted individuals revealed strong size- and density-dependence in demographic vital rates. For most sizes and vital rates, shrub density had negative demographic effects; there was no strong evidence for positive density dependence in any demographic process at any size. Statistical support for size- and density-dependence is provided in Tables B1–B6, which provide AIC rankings for candidate models based on the complete data set.

Survival. Among naturally occurring plants, survival of large, established individuals was very high (Fig. 2A). We observed relatively few mortality events and nearly all of these were among new recruits. The probability of survival at these small sizes declined with increasing density. Survival of transplants was very low, lower even than survival of similarly-sized, naturally occurring recruits (Fig. 2A). However, the transplant results support the general pattern of negative density dependence in survival. Among the 20 survivors, 15 of them occurred in transect windows below the median of weighted shrub density. In Appendix B, we show that transplant mortality was dominated by negative effects of shrub density at the 5-m window scale, even when effects of local grass and shrub cover were included as alternative or additional statistical covariates, which suggests that this is the appropriate spatial scale for modeling density dependence in this system.

474 *Growth.* Current size was strongly predictive of future size, as expected, and there was
475 weak negative density dependence in mean future size conditioned on current size (Fig.
476 2B). However, there was a stronger signal of density dependence in the variance of future
477 size (Fig. 2B, inset). Plants at low density exhibited greater variance in growth trajectories
478 and this was especially true at the smallest sizes. Thus, large increases (and decreases)
479 in the size of new recruits were most likely to occur under low-density conditions.

480 *Flowering and fruit production.* Flowering probability was strongly size-dependent and
481 and very weakly sensitive to local density (Fig. 2C). However, fertility of flowering plants
482 was strongly negative density dependent, with greatest flower and fruit production by
483 the largest plants at the lowest densities, and vice versa (Fig. 2D).

484 *Recruitment and recruit size.* We observed 32 natural recruitment events along our tran-
485 sects during the study years and our estimated recruitment rate, given total expected
486 seed production in each window preceding the recruitment year, was very low ($2.47 \times$
487 10^{-6} , 2E). While most recruitment events occurred at low density, this is also where
488 most seed production was concentrated (Fig. 2E), and low-density windows were over-
489 represented relative to high density. For these reasons we were more likely to observe re-
490 cruiment events at low density. Controlling for sampling effort and seed production, the
491 statistical models indicated that our data were most consistent with a constant, density-
492 independent seed-to-seedling recruitment rate (Table B5). However, the mean size of
493 new recruits declined significantly with local density (Fig. 2F).

494 *Population growth rate.* As expected given the vital rate results, the asymptotic popula-
495 tion growth rate λ declined monotonically with density (Fig. 3). This was true across
496 $> 98\%$ of bootstrap replicates, indicating high certainty that shrub fitness is maximized at

497 zero density and thus that the expansion wave is “pulled” (for this reason our wavespeed
498 results are based on the analytical approach described above). Mean growth rate at low
499 density was *ca.* 3% per year, with bootstrap uncertainty spanning 1–6%. At high density
500 in the core of the expansion wave, population growth rates approached $\lambda = 1$, indicating
501 population stasis driven by near-immortality and extremely rare recruitment.

502 *What is the seed dispersal kernel and how does it vary with maternal*
503 *plant size?*

504 WALD dispersal kernels were modeled using the properties of seeds and wind and
505 accounted for observed variation in wind speed, seed terminal velocity, and within-plant
506 seed release height. The resulting kernels were predicted to be strongly size dependent,
507 with taller plants having a greater probability of dispersing seeds longer distances (Fig.
508 4). However, predicted seed dispersal was highly local, with most seeds expected to
509 fall within one meter of parent plants for most sizes. Even for the very tallest shrub
510 we observed (1.96 m), only 6.2% of its seeds were predicted to fall more than 3 m away
511 and less than 1% were predicted to fall more than 6 m away (Fig. 4). Taller shrubs
512 also exhibited wider variance in their dispersal kernel, reflecting their wider range of
513 within-shrub seed release heights.

514 *What is the predicted rate of expansion and which lower-level processes*
515 *most strongly affect the expansion speed?*

516 The asymptotic speed of creosotebush encroachment, given the above demography and
517 dispersal patterns, was very slow. The mean asymptotic speed was 0.08 m/year and
518 the 5th–95th percentiles of the uncertainty distribution was 0.06–0.12 m/year (Fig. 5A).

519 The sensitivities of wavespeed spanned orders of magnitude, indicating strong unequal-
520 ity in the relative importance of the demography and dispersal processes controlling
521 expansion (Fig. 5B). Expansion speed was by far the most sensitive to the probability
522 of seedling recruitment (Fig. 5B), indicating that this life cycle transition imposes the
523 strongest constraint on encroachment. Sensitivity to survival ranked second, and since
524 nearly all mortality occurred at the smallest sizes this too can be interpreted as an early
525 life cycle constraint on expansion. The mean of growth ranked third and this was also
526 likely related to early plant survival, since increases in size allow small plants to reach
527 “protected” sizes given the strong size-dependence in survival.

528 *How does the observed rate of encroachment in the recent past compare to*
529 *model predictions?*

530 Re-surveys along two permanent transects revealed virtually no change the in the cre-
531 osotebush expansion wave over the 12 years that preceded our study (Fig. 6). There
532 were local changes in percent cover suggesting that shrubs were filling habitat behind
533 the wave from: 58% of patches had non-zero cover of creosotebush in 2001 compared to
534 65% in 2013. However, there was no clear indication that the leading edge of the shrub-
535 land has advanced (the modest right-ward shift on both transects is within the range of
536 measurement error).

537 **Discussion**

538 The encroachment of grasslands by woody plants is a worldwide phenomenon with
539 broad implications for biodiversity and ecosystem function. A theoretical perspective
540 rooted in spatial population biology brings attention to the combined influence of dis-

persal and density-dependent demography as critical controls on the occurrence and pace of encroachment. Through this lens, we asked whether the encroachment process is pushed or pulled, hypothesizing that potential for positive feedbacks may cause declines in fitness at the low-density front and generate pushed-wave dynamics. Instead, observational and experimental evidence indicate that fitness was maximized in low-density plant neighborhoods. The creosotebush encroachment wave is therefore predicted to be pulled by maximum demographic performance at the leading edge. However, our field-parameterized spatial integral projection model revealed that this wave is pulled at the very slow rate of 6–12 centimeters per year – so slow that, under the observed conditions, this grass-shrub ecotone is effectively stationary. In fact, to our knowledge, this is the slowest plant population wavespeed estimated using SIPMs or their matrix model progenitors (Neubert and Caswell, 2000). Re-surveys of permanent transects independently supported this prediction, showing virtually no change in the position of the shrub boundary in over a decade. Creosotebush has a well documented history of expansion throughout the Southwest US, so it is clearly capable of rapid invasion. Yet, whatever historical conditions allowed for shrub encroachment to its current extent, the encroachment wave at SNWR is presently stalled, under the conditions we observed it. Below, we discuss and interpret these key findings and their broader implications in greater detail.

Observational and experimental evidence strongly indicated that effects of shrub density were strongly negative in all vital rates and at all sizes. This was surprising given widespread evidence for positive feedbacks (which should generate low-density fitness penalties) in woody plant encroachment generally (D’odorico et al., 2013) and specifically in our creosotebush system (D’Odorico et al., 2010). How can we square these apparently conflicting results? First, it may be important to consider the distinction be-

566 tween “demographic” and “component” Allee effects (Stephens et al., 1999), which refer
567 to effects that manifest in total fitness and components of fitness, respectively. That is,
568 positive effects of conspecific density may occur, but in our measures of demographic
569 performance these are swamped by stronger, counter-acting negative effects. It is worth
570 noting that our demographic measurements are temporally coarse, reflecting aggregate
571 performance over a full transition year. More mechanistic studies on finer time scales
572 might reveal component Allee effects that are masked by strong net-negative density
573 dependence. Second, many of the potential mechanisms for positive feedbacks at shrub-
574 grass ecotones would manifest infrequently. For example, effects of shrub encroachment
575 on microclimate (D’odorico et al., 2013) may promote shrub survival only in the face of
576 rare climate events such as extreme low temperatures. Similarly, positive feedbacks that
577 occur via fire suppression (Collins et al., 2021; Ratajczak et al., 2011) would only manifest
578 on timescales that are inclusive of fire return intervals. These considerations suggest that
579 we may be more likely to detect positive density dependence over longer time scales
580 encompassing conditions that trigger positive feedbacks. This leads to the hypothesis
581 that the shrub encroachment wave is *usually* pulled but occasionally pushed. To our
582 knowledge such switches have never been empirically documented in any expanding
583 population but may be an important feature of expansion in fluctuating environments.

584 The very low transplant survival and recruitment rates that we measured also call at-
585 tention to time scale. Previous studies suggest that creosotebush recruitment is strongly
586 episodic, likely in response to large, infrequent monsoon precipitation events (Allen
587 et al., 2008; Boyd and Brum, 1983; Moreno-de las Heras et al., 2016). Similar patterns
588 of episodic recruitment driven by large precipitation events have been observed in other
589 cases of woody plant encroachment in aridlands (Harrington, 1991; Weber-Grullon et al.,
590 2022), and relatively high transplant survival on the one transect that we planted im-

591 mediately following a large monsoon event anecdotally supports an important role for
592 soil moisture. With only four transition-years of demographic data, we chose to combine
593 information across years and build a deterministic model that averages over inter-annual
594 variability. However, the connection between shrub recruitment and monsoon precipita-
595 tion, combined with the observed and projected increase in the variability of monsoon
596 precipitation in our study region (Petrie et al., 2014; Rudgers et al., 2018), suggest that ex-
597 tending our deterministic model to accommodate inter-annual variability in climate and
598 climate-dependent vital rates will be a critical next step. Because our wavespeed esti-
599 mate is acutely sensitive to the seed-to-seedling transition, much more so than any other
600 demographic or dispersal process, we expect that a stochastic model incorporating many
601 years of data may yield a faster predicted expansion speed driven by rare pulses of re-
602 cruitment (Ellner and Schreiber, 2012). Such pulses have clearly not occurred during our
603 study years (2013–2017) or the preceding decade of transect re-surveys (2001–2012) and
604 therefore we think the deterministic model is an adequate representation of the observed
605 conditions. However, our findings of pulled-wave dynamics and strong wavespeed sen-
606 sitivity to seedling recruitment indicate that the present shrub ecotone is primed for
607 expansion once the necessary climate conditions align, as they likely will in a more
608 variable climate regime. While monsoon precipitation is a leading candidate for factors
609 promoting seedling establishment, it is worth noting that our study years included both
610 the lowest and second-highest amounts of monsoon precipitation in a 20-year record,
611 and yet these events did not correlate with seedling recruitment on our transects (Fig.
612 B1). The conditions favoring recruitment and recruit survival may therefore be more
613 complicated than the single driver of monsoon precipitation.

614 While not as strong a constraint as recruitment based on our sensitivity analysis, lim-
615 ited dispersal ability also contributed to the very slow predicted speed of encroachment.

Our findings of very limited dispersal are consistent with a previous study that found creosotebush seeds in the seed bank were found only beneath mature shrubs and not in nearby grass patches or inter-plant spaces (Moreno-de las Heras et al., 2016). Our mechanistic dispersal modeling assumes that wind is the sole dispersal vector. Previous work suggests that this modeling approach can accurately predict dispersal patterns for wind-dispersed plants (Skarpaas and Shea, 2007), yet in our system it may be important to consider secondary dispersal vectors. Boyd and Brum's 1983 study of creosotebush reproductive biology described "contradiction in the literature about mode of dispersal", citing evidence for a dominant role of wind but the additional possibility of seed movement by granivorous animals. Combining wind and animal dispersal vectors into a "total" dispersal kernel (Rogers et al., 2019) will be a valuable next step. Second, overland flow of runoff may contribute to secondary seed movement following initial deposition by wind (Thompson et al., 2014). Interestingly, seed movement from overland flow would be most likely following large monsoon events. Therefore the same conditions that promote seedling recruitment may also promote long-distance dispersal, potentially amplifying a pulse of shrub encroachment (Ellner and Schreiber, 2012). Seeds may also be blown along the ground following initial deposition, which our model does not account for. The classic WALD dispersal model employed here assumes uniform grass cover, with seeds trapped below the height of this grass canopy. As in aridlands worldwide, our northern Chihuahuan Desert study region is characterized by a high percentage of bare ground, especially in areas of high creosotebush density (Fig. 1). New approaches are needed to extend mechanistic dispersal modeling to accommodate this feature of aridlands, as others have recognized (Thompson et al., 2014). The potential roles for both biotic and abiotic secondary dispersal vectors makes our dispersal kernel a conservative estimate of seed movement and highlights a need for further study of shrub

641 seed dispersal.

642 Our model focused on intra-specific density dependence but inter-specific plant-plant
643 interactions may be an important element of shrub encroachment. For example, over-
644 grazing is a hypothesized driver of shrub encroachment due to release from grass com-
645 petition and reduction of grassland fires (Van Auken, 2000). Our shrub encroachment
646 model considered only one “side” of the grass-shrub ecotone, assuming that the shrub
647 population spreads into empty space. Explicit consideration of grass competition or facil-
648 itation may enrich our understanding of shrub expansion or lack thereof in this and other
649 systems. However, our transplant experiment suggested weak negative effects of grass
650 cover on seedling survival (Figure C1B). Similarly, grass competition had no effect on
651 germination and survival of mesquite (*Prosopis glandulosa*) shrubs in Chihuahuan Desert
652 grassland (Weber-Grullon et al., 2022). While our current data do not allow us to quan-
653 tify whether and how strongly resident grasses may slow down shrub encroachment,
654 we can infer that competitive effects of grasses on shrubs are weaker than competitive
655 effects of shrubs on shrubs. Therefore our conclusion that the encroachment wave is
656 pulled implicitly accounts for any effects of grass cover.

657 While our data reveal strong negative density dependence, we know little about the
658 underlying mechanisms that give rise to this pattern. What is it about high shrub density
659 environments that suppress survival and reproduction? The abundance of bare ground
660 in core shrubland suggests that shrubs do not compete for space. However, Brisson
661 and Reynolds (1994) found strong competition for space belowground, with crowded
662 neighborhoods constraining creosotebush root systems. Also, root development of cre-
663 osotebush seedlings can respond rapidly to the availability of soil moisture (Obrist and
664 Arnone III, 2003), suggesting that competition for water may be another element of den-
665 sity dependence. Finally, negative density dependence in plants may also be mediated by

666 consumers or soil microbes. Better understanding the environmental drivers of density
667 dependence will enable better prediction for how the encroachment wave may respond
668 to future environmental change.

669 *Conclusions.* Understanding and predicting the dynamics of woody-herbaceous eco-
670 tones requires that we build knowledge of the fates of the rare individuals that disperse
671 from core habitat and cross habitat boundaries. For a creosotebush, there is no better
672 place to be than alone in a grassland, and that key result governs the spatial dynamics of
673 this population. We found that wave of creosotebush expansion into Chihuahuan desert
674 grassland is pulled by peak fitness at the leading edge. However, it is pulled so slowly
675 that it is effectively stalled, a model-derived prediction that is supported by independent
676 data. Had we only relied on the re-survey data without insight from the mechanistic
677 model we might have concluded that the creosotebush ecotone is stable at its current
678 boundary. Instead, acute sensitivity of a slow wave to seedling recruitment leaves this
679 system poised for pulses of expansion under the right conditions; what exactly those
680 conditions are is not yet fully resolved. We suggest that the concepts and tools of spatial
681 population biology may facilitate advances in the study and management of woody plant
682 encroachment, which, like all spreading populations, must be driven by birth, death, and
683 movement.

684 **Acknowledgements**

685 This research was supported by the Sevilleta LTER program (NSF DEB awards 1655499,
686 1748133) and by NSF DEB award 1856383. We are grateful to Andrew Bibian, Aldo Com-
687 pagnoni, Kevin Czachura, Marion Donald, Kory Kolis, Johanna Ohm, Rande Patterson,
688 Eréndira Quintana Morales, Olivia Ragni, Emily Schultz, and Charlene Thomas for their

689 contributions to field data collection. Kat Shea and Olav Skarpaas provided helpful guid-
690 ance on dispersal modeling. This research was permitted by the US Fish and Wildlife
691 Service with a Special Use Permit.

692 **Author contributions**

693 All authors contributed to study design. THD and TEXM led data analysis, modeling,
694 and writing early drafts of the manuscript. All authors participated in preparing the
695 manuscript for submission.

696 **Literature Cited**

- 697 Allen, A., W. Pockman, C. Restrepo, and B. Milne. 2008. Allometry, growth and pop-
698 ulation regulation of the desert shrub *Larrea tridentata*. *Functional Ecology* pages
699 197–204.
- 700 Bowers, J. E., R. M. Turner, and T. L. Burgess. 2004. Temporal and spatial patterns in
701 emergence and early survival of perennial plants in the Sonoran Desert. *Plant Ecology*
702 **172**:107–119.
- 703 Boyd, R. S., and G. D. Brum. 1983. Postdispersal reproductive biology of a Mojave Desert
704 population of *Larrea tridentata* (Zygophyllaceae). *American Midland Naturalist* pages
705 25–36.
- 706 Brandt, J. S., M. A. Haynes, T. Kuemmerle, D. M. Waller, and V. C. Radeloff. 2013.
707 Regime shift on the roof of the world: Alpine meadows converting to shrublands in
708 the southern Himalayas. *Biological Conservation* **158**:116–127.

- 709 Brisson, J., and J. F. Reynolds. 1994. The effect of neighbors on root distribution in a
710 creosotebush (*Larrea tridentata*) population. *Ecology* **75**:1693–1702.
- 711 Buffington, L. C., and C. H. Herbel. 1965. Vegetational changes on a semidesert grassland
712 range from 1858 to 1963. *Ecological monographs* **35**:139–164.
- 713 Bullock, J. M., S. M. White, C. Prudhomme, C. Tansey, R. Perea, and D. A. Hooftman.
714 2012. Modelling spread of British wind-dispersed plants under future wind speeds in
715 a changing climate. *Journal of Ecology* **100**:104–115.
- 716 Cabral, A., J. De Miguel, A. Rescia, M. Schmitz, and F. Pineda. 2003. Shrub encroachment
717 in Argentinean savannas. *Journal of Vegetation Science* **14**:145–152.
- 718 Collins, S. L., J. B. Nippert, J. M. Blair, J. M. Briggs, P. Blackmore, and Z. Ratajczak.
719 2021. Fire frequency, state change and hysteresis in tallgrass prairie. *Ecology Letters*
720 **24**:636–647.
- 721 D’Odorico, P., J. D. Fuentes, W. T. Pockman, S. L. Collins, Y. He, J. S. Medeiros,
722 S. DeWekker, and M. E. Litvak. 2010. Positive feedback between microclimate and
723 shrub encroachment in the northern Chihuahuan desert. *Ecosphere* **1**:1–11.
- 724 D’odorico, P., Y. He, S. Collins, S. F. De Wekker, V. Engel, and J. D. Fuentes. 2013.
725 Vegetation–microclimate feedbacks in woodland–grassland ecotones. *Global Ecology*
726 *and Biogeography* **22**:364–379.
- 727 D’Odorico, P., G. S. Okin, and B. T. Bestelmeyer. 2012. A synthetic review of feedbacks
728 and drivers of shrub encroachment in arid grasslands. *Ecohydrology* **5**:520–530.
- 729 Duran, K. L., T. K. Lowrey, R. R. Parmenter, and P. O. Lewis. 2005. Genetic diversity in
730 Chihuahuan Desert populations of creosotebush (*Zygophyllaceae*: *Larrea tridentata*).
731 *American Journal of Botany* **92**:722–729.

- 732 Ellner, S. P., D. Z. Childs, M. Rees, et al. 2016. Data-driven modelling of structured
733 populations. A practical guide to the Integral Projection Model. Cham: Springer .
- 734 Ellner, S. P., and S. J. Schreiber. 2012. Temporally variable dispersal and demography can
735 accelerate the spread of invading species. *Theoretical Population Biology* **82**:283–298.
- 736 Gandhi, S. R., E. A. Yurtsev, K. S. Korolev, and J. Gore. 2016. Range expansions transition
737 from pulled to pushed waves as growth becomes more cooperative in an experimental
738 microbial population. *Proceedings of the National Academy of Sciences* **113**:6922–6927.
- 739 Gardner, J. L. 1951. Vegetation of the creosotebush area of the Rio Grande Valley in New
740 Mexico. *Ecological Monographs* **21**:379–403.
- 741 Gibbens, R., R. McNeely, K. Havstad, R. Beck, and B. Nolen. 2005. Vegetation changes in
742 the Jornada Basin from 1858 to 1998. *Journal of Arid Environments* **61**:651–668.
- 743 Goslee, S., K. Havstad, D. Peters, A. Rango, and W. Schlesinger. 2003. High-resolution
744 images reveal rate and pattern of shrub encroachment over six decades in New Mexico,
745 USA. *Journal of Arid Environments* **54**:755–767.
- 746 Grover, H. D., and H. B. Musick. 1990. Shrubland encroachment in southern New Mex-
747 ico, USA: an analysis of desertification processes in the American Southwest. *Climatic*
748 *change* **17**:305–330.
- 749 Harrington, G. N. 1991. Effects of soil moisture on shrub seedling survival in semi-arid
750 grassland. *Ecology* **72**:1138–1149.
- 751 Hsieh, C.-I., and G. G. Katul. 1997. Dissipation methods, Taylor’s hypothesis, and
752 stability correction functions in the atmospheric surface layer. *Journal of Geophysical*
753 *Research: Atmospheres* **102**:16391–16405.

- 754 Huang, H., L. D. Anderegg, T. E. Dawson, S. Mote, and P. D’Odorico. 2020. Critical tran-
755 sition to woody plant dominance through microclimate feedbacks in North American
756 coastal ecosystems. *Ecology* **101**:e03107.
- 757 Jongejans, E., K. Shea, O. Skarpaas, D. Kelly, and S. P. Ellner. 2011. Importance of
758 individual and environmental variation for invasive species spread: a spatial integral
759 projection model. *Ecology* **92**:86–97.
- 760 Katul, G., A. Porporato, R. Nathan, M. Siqueira, M. Soons, D. Poggi, H. Horn, and S. A.
761 Levin. 2005. Mechanistic analytical models for long-distance seed dispersal by wind.
762 *The American Naturalist* **166**:368–381.
- 763 Keitt, T. H., M. A. Lewis, and R. D. Holt. 2001. Allee effects, invasion pinning, and
764 species’ borders. *The American Naturalist* **157**:203–216.
- 765 Kelleway, J. J., K. Cavanaugh, K. Rogers, I. C. Feller, E. Ens, C. Doughty, and N. Saintilan.
766 2017. Review of the ecosystem service implications of mangrove encroachment into
767 salt marshes. *Global Change Biology* **23**:3967–3983.
- 768 Knapp, A. K., J. M. Briggs, S. L. Collins, S. R. Archer, M. S. BRET-HARTE, B. E. Ewers,
769 D. P. Peters, D. R. Young, G. R. Shaver, E. Pendall, et al. 2008. Shrub encroachment in
770 North American grasslands: shifts in growth form dominance rapidly alters control of
771 ecosystem carbon inputs. *Global Change Biology* **14**:615–623.
- 772 Kot, M., M. A. Lewis, and P. van den Driessche. 1996. Dispersal data and the spread of
773 invading organisms. *Ecology* **77**:2027–2042.
- 774 Lewis, M., and P. Kareiva. 1993. Allee dynamics and the spread of invading organisms.
775 *Theoretical Population Biology* **43**:141–158.

- 776 Lewis, M. A., M. G. Neubert, H. Caswell, J. S. Clark, and K. Shea, 2006. A guide to cal-
 777 culating discrete-time invasion rates from data. Pages 169–192 *in* Conceptual ecology
 778 and invasion biology: reciprocal approaches to nature. Springer.
- 779 Mabry, T. J., J. H. Hunziker, D. Difeo Jr, et al. 1978. Creosote bush: biology and chemistry
 780 of *Larrea* in New World deserts. Dowden, Hutchinson & Ross, Inc.
- 781 Maddox, J. C., and S. Carlquist. 1985. Wind dispersal in Californian desert plants:
 782 experimental studies and conceptual considerations. *Aliso: A Journal of Systematic*
 783 *and Evolutionary Botany* **11**:77–96.
- 784 McAuliffe, J., E. Hamerlynck, and M. Eppes. 2007. Landscape dynamics fostering the
 785 development and persistence of long-lived creosotebush (*Larrea tridentata*) clones in
 786 the Mojave Desert. *Journal of Arid Environments* **69**:96–126.
- 787 Moore, D., and K. Hall, 2022. Meteorology Data from the Sevilleta Na-
 788 tional Wildlife Refuge, New Mexico. Environmental Data Initiative.
 789 <https://doi.org/10.6073/pasta/d56307b398e28137dabaa6994f0f5f92>.
- 790 Moreno-de las Heras, M., L. Turnbull, and J. Wainwright. 2016. Seed-bank structure
 791 and plant-recruitment conditions regulate the dynamics of a grassland-shrubland Chi-
 792 huahuan ecotone. *Ecology* **97**:2303–2318.
- 793 Mugasi, S., E. Sabiiti, and B. Tayebwa. 2000. The economic implications of bush en-
 794 croachment on livestock farming in rangelands of Uganda. *African Journal of Range*
 795 *and Forage Science* **17**:64–69.
- 796 Nathan, R., G. G. Katul, G. Bohrer, A. Kuppinen, M. B. Soons, S. E. Thompson, A. Trakht-
 797 enbrot, and H. S. Horn. 2011. Mechanistic models of seed dispersal by wind. *Theoret-*
 798 *ical Ecology* **4**:113–132.

- 799 Neubert, M. G., and H. Caswell. 2000. Demography and dispersal: calculation and
800 sensitivity analysis of invasion speed for structured populations. *Ecology* **81**:1613–
801 1628.
- 802 Oba, G., E. Post, P. Syvertsen, and N. Stenseth. 2000. Bush cover and range condition
803 assessments in relation to landscape and grazing in southern Ethiopia. *Landscape*
804 *ecology* **15**:535–546.
- 805 Obrist, D., and J. Arnone III. 2003. Increasing CO₂ accelerates root growth and enhances
806 water acquisition during early stages of development in *Larrea tridentata*. *New Phy-*
807 *tologist* **159**:175–184.
- 808 Pan, S., and G. Lin. 2012. Invasion traveling wave solutions of a competitive system with
809 dispersal. *Boundary Value Problems* **2012**:120.
- 810 Parizek, B., C. M. Rostagno, and R. Sottini. 2002. Soil erosion as affected by shrub
811 encroachment in northeastern Patagonia. *Rangeland Ecology & Management/Journal*
812 *of Range Management Archives* **55**:43–48.
- 813 Peters, D. P., and J. Yao. 2012. Long-term experimental loss of foundation species:
814 consequences for dynamics at ecotones across heterogeneous landscapes. *Ecosphere*
815 **3**:1–23.
- 816 Petrie, M., S. Collins, D. Gutzler, and D. Moore. 2014. Regional trends and local vari-
817 ability in monsoon precipitation in the northern Chihuahuan Desert, USA. *Journal of*
818 *Arid Environments* **103**:63–70.
- 819 Ratajczak, Z., J. B. Nippert, and S. L. Collins. 2012. Woody encroachment decreases
820 diversity across North American grasslands and savannas. *Ecology* **93**:697–703.

- 821 Ratajczak, Z., J. B. Nippert, J. C. Hartman, and T. W. Ocheltree. 2011. Positive feedbacks
822 amplify rates of woody encroachment in mesic tallgrass prairie. *Ecosphere* **2**:1–14.
- 823 Raupach, M. 1994. Simplified expressions for vegetation roughness length and zero-
824 plane displacement as functions of canopy height and area index. *Boundary-Layer*
825 *Meteorology* **71**:211–216.
- 826 Ravi, S., P. D’Odorico, S. L. Collins, and T. E. Huxman. 2009. Can biological invasions
827 induce desertification? *The New Phytologist* **181**:512–515.
- 828 Reed, M., L. Stringer, A. Dougill, J. Perkins, J. Atlhopheng, K. Mulale, and N. Favretto.
829 2015. Reorienting land degradation towards sustainable land management: Linking
830 sustainable livelihoods with ecosystem services in rangeland systems. *Journal of envi-*
831 *ronmental management* **151**:472–485.
- 832 Reynolds, J. F., R. A. Virginia, P. R. Kemp, A. G. De Soyza, and D. C. Tremmel. 1999.
833 Impact of drought on desert shrubs: effects of seasonality and degree of resource
834 island development. *Ecological Monographs* **69**:69–106.
- 835 Rogers, H. S., N. G. Beckman, F. Hartig, J. S. Johnson, G. Pufal, K. Shea, D. Zurell, J. M.
836 Bullock, R. S. Cantrell, B. Loiselle, et al. 2019. The total dispersal kernel: a review and
837 future directions. *AoB Plants* **11**:plz042.
- 838 Roques, K., T. O’connor, and A. R. Watkinson. 2001. Dynamics of shrub encroachment in
839 an African savanna: relative influences of fire, herbivory, rainfall and density depen-
840 dence. *Journal of Applied Ecology* **38**:268–280.
- 841 Rudgers, J. A., Y. A. Chung, G. E. Maurer, D. I. Moore, E. H. Muldavin, M. E. Litvak,
842 and S. L. Collins. 2018. Climate sensitivity functions and net primary production: a
843 framework for incorporating climate mean and variability. *Ecology* **99**:576–582.

- 844 Schlesinger, W. H., and A. M. Pilmanis. 1998. Plant-soil interactions in deserts. *Biogeo-*
845 *chemistry* **42**:169–187.
- 846 Schlesinger, W. H., J. A. Raikes, A. E. Hartley, and A. F. Cross. 1996. On the spatial
847 pattern of soil nutrients in desert ecosystems: ecological archives E077-002. *Ecology*
848 **77**:364–374.
- 849 Schlesinger, W. H., J. F. Reynolds, G. L. Cunningham, L. F. Huenneke, W. M. Jarrell, R. A.
850 Virginia, and W. G. Whitford. 1990. Biological feedbacks in global desertification.
851 *Science* **247**:1043–1048.
- 852 Sirami, C., and A. Monadjem. 2012. Changes in bird communities in Swaziland savannas
853 between 1998 and 2008 owing to shrub encroachment. *Diversity and Distributions*
854 **18**:390–400.
- 855 Skarpaas, O., and K. Shea. 2007. Dispersal patterns, dispersal mechanisms, and invasion
856 wave speeds for invasive thistles. *The American Naturalist* **170**:421–430.
- 857 Stephens, P. A., W. J. Sutherland, and R. P. Freckleton. 1999. What is the Allee effect?
858 *Oikos* pages 185–190.
- 859 Sullivan, L. L., B. Li, T. E. Miller, M. G. Neubert, and A. K. Shaw. 2017. Density depen-
860 dence in demography and dispersal generates fluctuating invasion speeds. *Proceed-*
861 *ings of the National Academy of Sciences* **114**:5053–5058.
- 862 Taylor, C. M., and A. Hastings. 2005. Allee effects in biological invasions. *Ecology Letters*
863 **8**:895–908.
- 864 Thompson, S. E., S. Assouline, L. Chen, A. Trahktenbrot, T. Svoray, and G. G. Katul. 2014.
865 Secondary dispersal driven by overland flow in drylands: Review and mechanistic
866 model development. *Movement ecology* **2**:7.

- 867 Trollope, W., F. Hobson, J. Danckwerts, and J. Van Niekerk. 1989. Encroachment and
868 control of undesirable plants. *Veld management in the Eastern Cape* pages 73–89.
- 869 Turnbull, L., J. Wainwright, and R. E. Brazier. 2010. Changes in hydrology and erosion
870 over a transition from grassland to shrubland. *Hydrological Processes: An Interna-*
871 *tional Journal* **24**:393–414.
- 872 Van Auken, O. 2009. Causes and consequences of woody plant encroachment into
873 western North American grasslands. *Journal of environmental management* **90**:2931–
874 2942.
- 875 Van Auken, O. W. 2000. Shrub invasions of North American semiarid grasslands. *Annual*
876 *review of ecology and systematics* **31**:197–215.
- 877 Vasek, F. C. 1980. Creosote bush: Long-lived clones in the Mojave Desert. *American*
878 *Journal of Botany* **67**:246–255.
- 879 Veit, R. R., and M. A. Lewis. 1996. Dispersal, population growth, and the Allee effect: dy-
880 namics of the house finch invasion of eastern North America. *The American Naturalist*
881 **148**:255–274.
- 882 Wang, M.-H., M. Kot, and M. G. Neubert. 2002. Integrodifference equations, Allee effects,
883 and invasions. *Journal of mathematical biology* **44**:150–168.
- 884 Weber-Grullon, L., L. Gherardi, W. A. Rutherford, S. R. Archer, and O. E. Sala. 2022.
885 Woody-plant encroachment: Precipitation, herbivory, and grass-competition interact
886 to affect shrub recruitment. *Ecological Applications* **32**:e2536.
- 887 Wiernga, J. 1993. Representative roughness parameters for homogeneous terrain.
888 *Boundary-Layer Meteorology* **63**:323–363.

- 889 Wilcox, B. P., A. Birt, S. D. Fuhlendorf, and S. R. Archer. 2018. Emerging frameworks for
890 understanding and mitigating woody plant encroachment in grassy biomes. *Current*
891 *Opinion in Environmental Sustainability* **32**:46–52.
- 892 Williams, J. L., T. E. Miller, and S. P. Ellner. 2012. Avoiding unintentional eviction from
893 integral projection models. *Ecology* **93**:2008–2014.
- 894 Wood, S. 2017. *Generalized Additive Models: An Introduction with R*. 2 edition. Chap-
895 man and Hall/CRC.

Figure legends

Figure 1. Example of an ecotone transect spanning gradients of creosotebush and black grama grass at Sevilleta National Wildlife Refuge, a Long-Term Ecological Research (LTER) site in central New Mexico, US.

Figure 2. Size- and density-dependence in demographic vital rates. **A** Probability of survival from natural population census and transplant experiment (black line), **B** Mean and variance (inset) of size conditional on previous size, **C** Probability of flowering, **D** Flower and fruit production, **E** Probability of recruitment per seed, **F** Recruit size. In **A–D**, colored lines indicate four size groups (red is largest, blue is smallest), discretized for data visualization only. In all panels, weighted density is the sum of all plant sizes $\log(\text{cm}^3)$ within the same 5-m window as the census individual.

Figure 3. Density dependence in the asymptotic population growth rate (λ). Gray lines show bootstrap replicates and the black lines shows predictions from full demographic data set. Weighted density is the sum of all plant sizes $\log(\text{cm}^3)$ within 5-m windows.

Figure 4. Predicted WALD dispersal kernels for four shrub heights corresponding to the 25th, 50th, 75th, and 100th (maximum) percentiles of the observed size distribution. We assume that heights below 15 cm have effectively no seed movement due to interference with the grass layer.

Figure 5. **A**, Asymptotic speed of creosotebush encroachment. The distribution reflects parameter and model uncertainties quantified via bootstrapping and stochastic sampling from seed dispersal kernels. **B**, Sensitivities of wavespeed to demography and dispersal processes. For size-dependent functions (growth, survival, flowering, and fertility) sensitivity was calculated by perturbing the entire function across all sizes.

⁹²⁰ **Figure 6.** Surveys of creosotebush percent cover along two permanent transects (A,B) in
⁹²¹ 2001 and 2013.

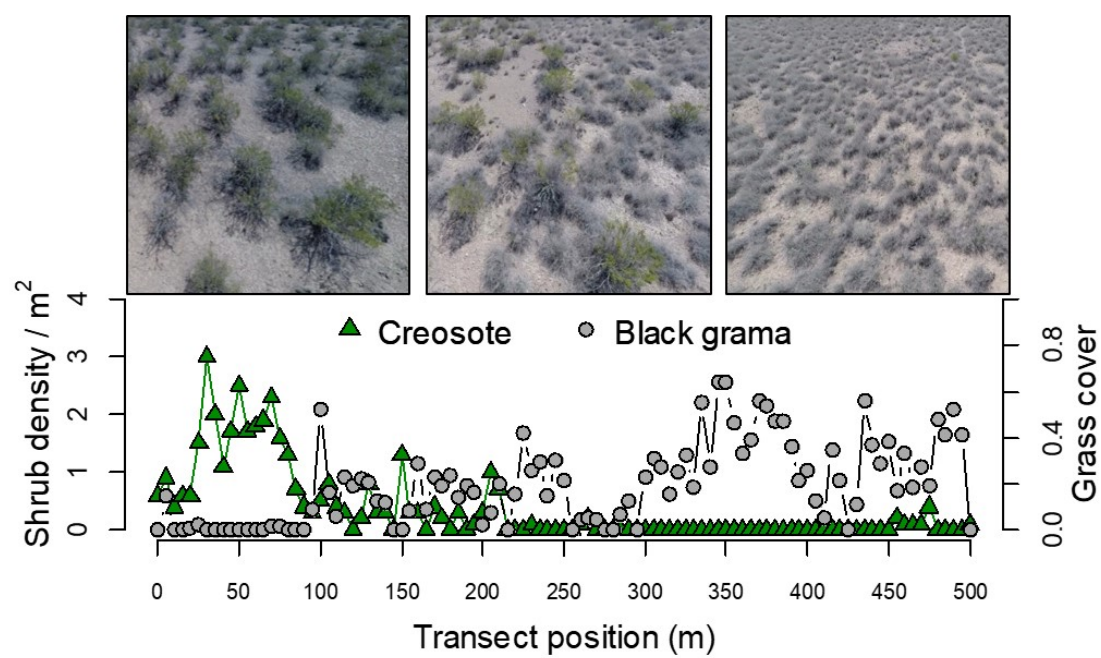


Figure 1

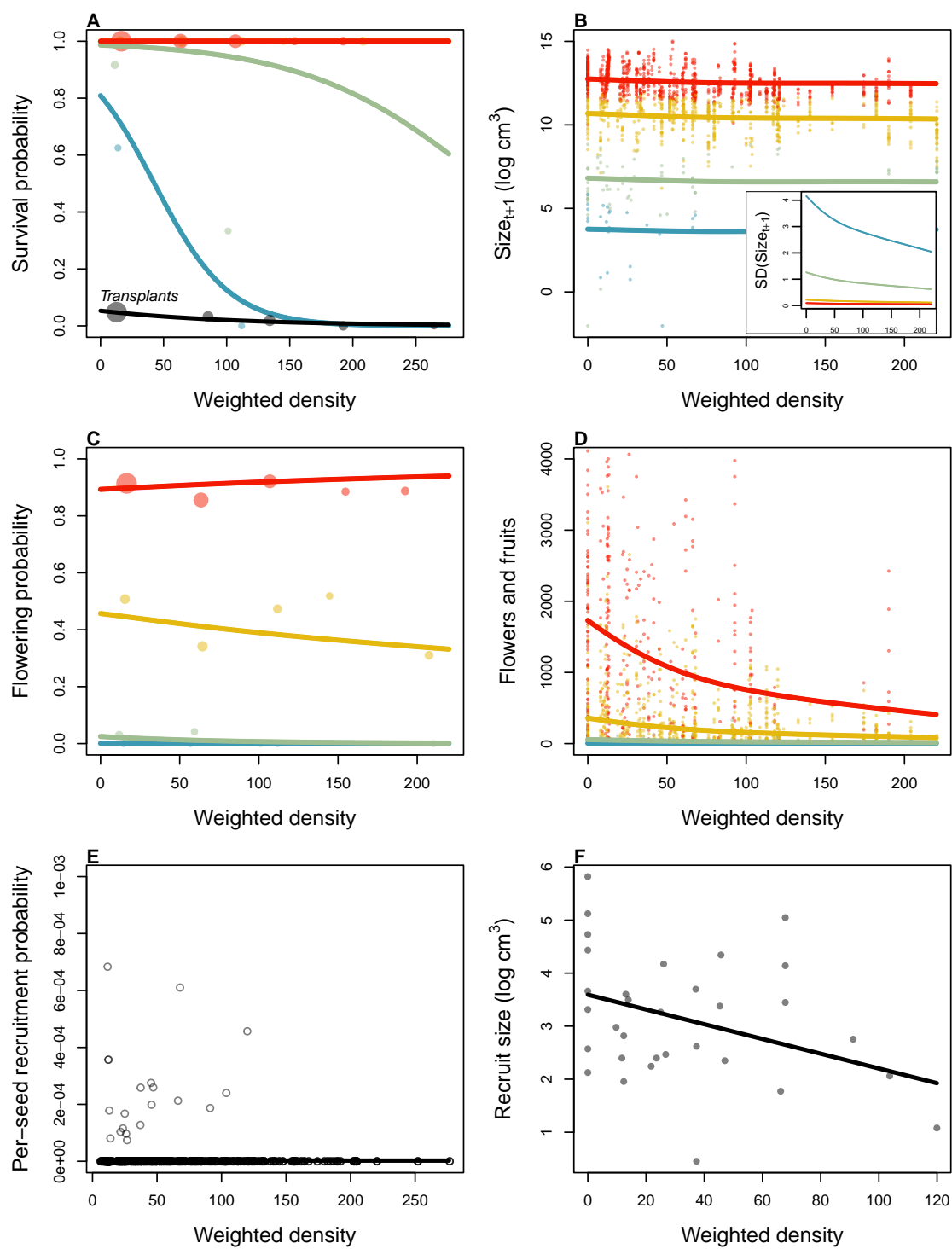


Figure 2

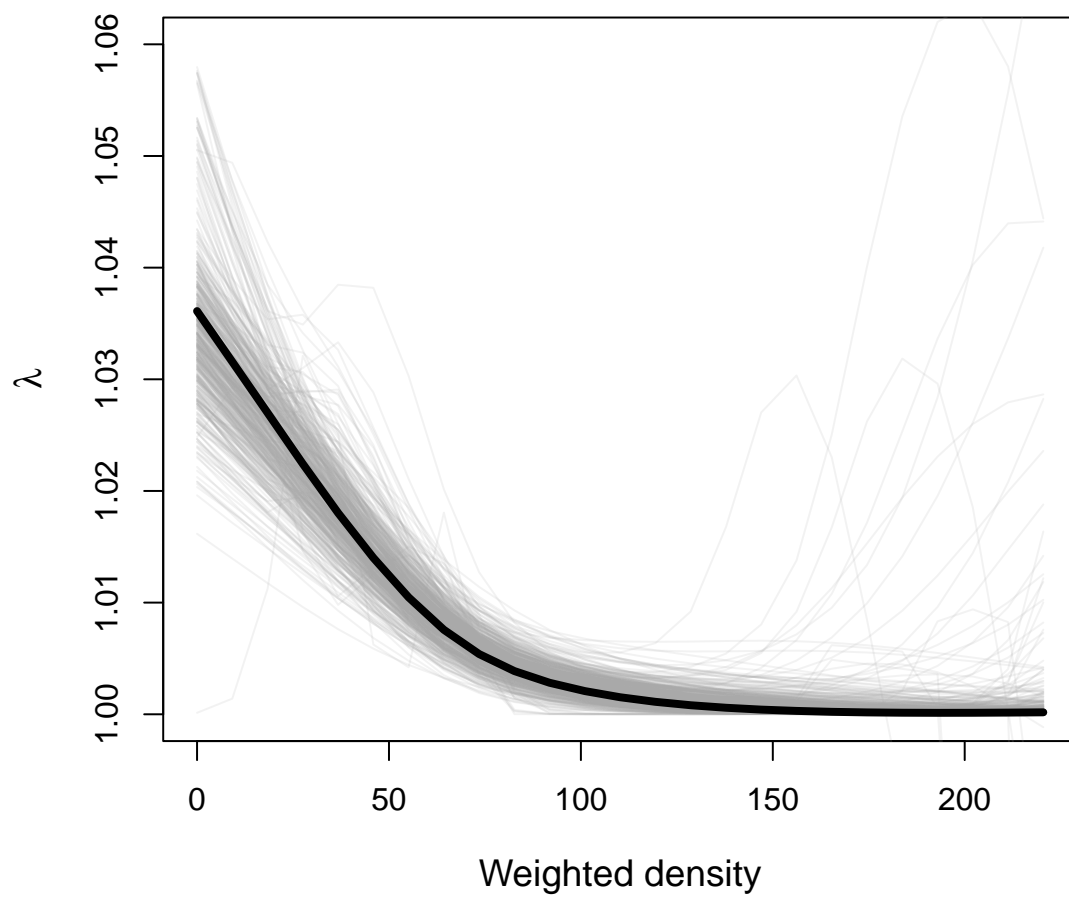


Figure 3

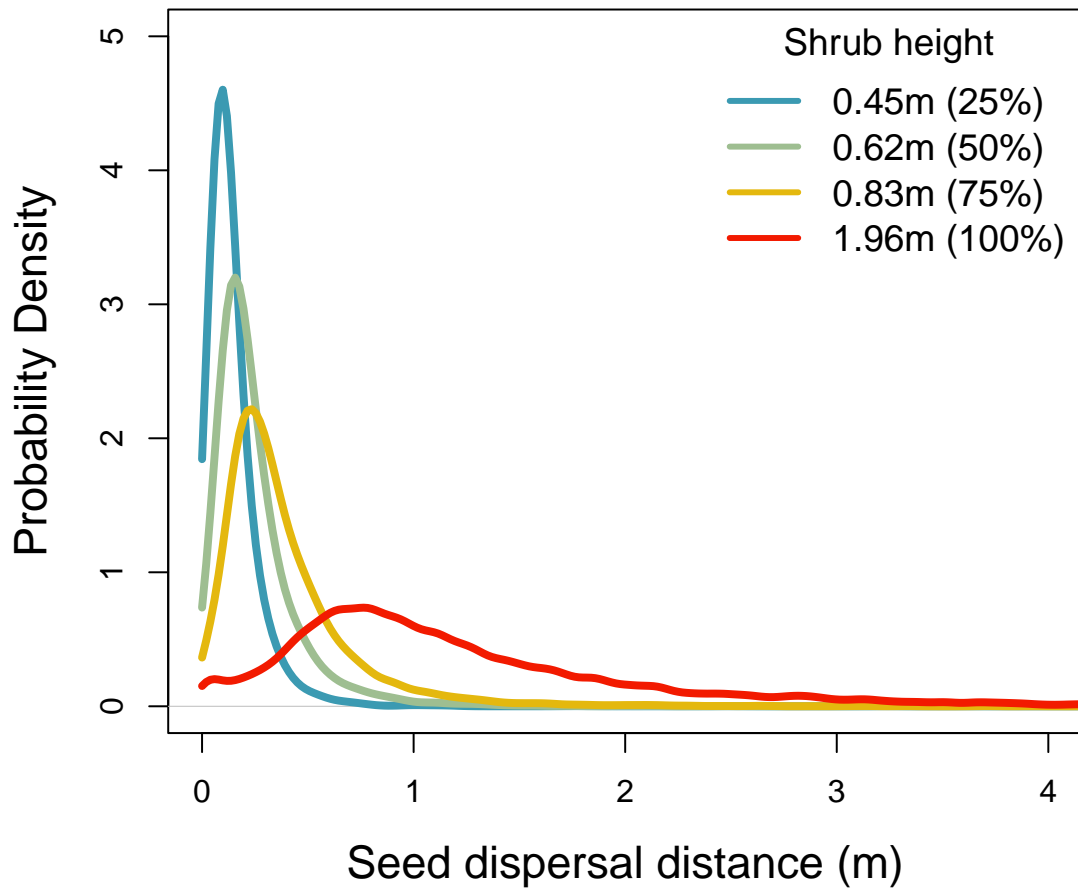


Figure 4

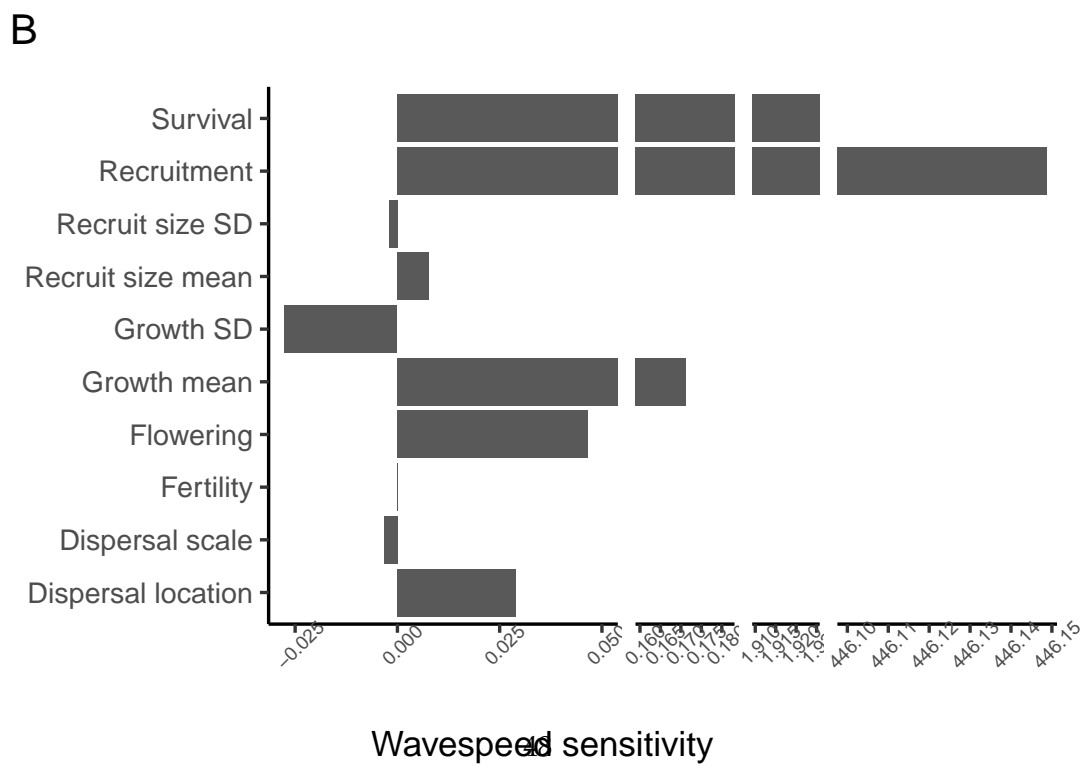
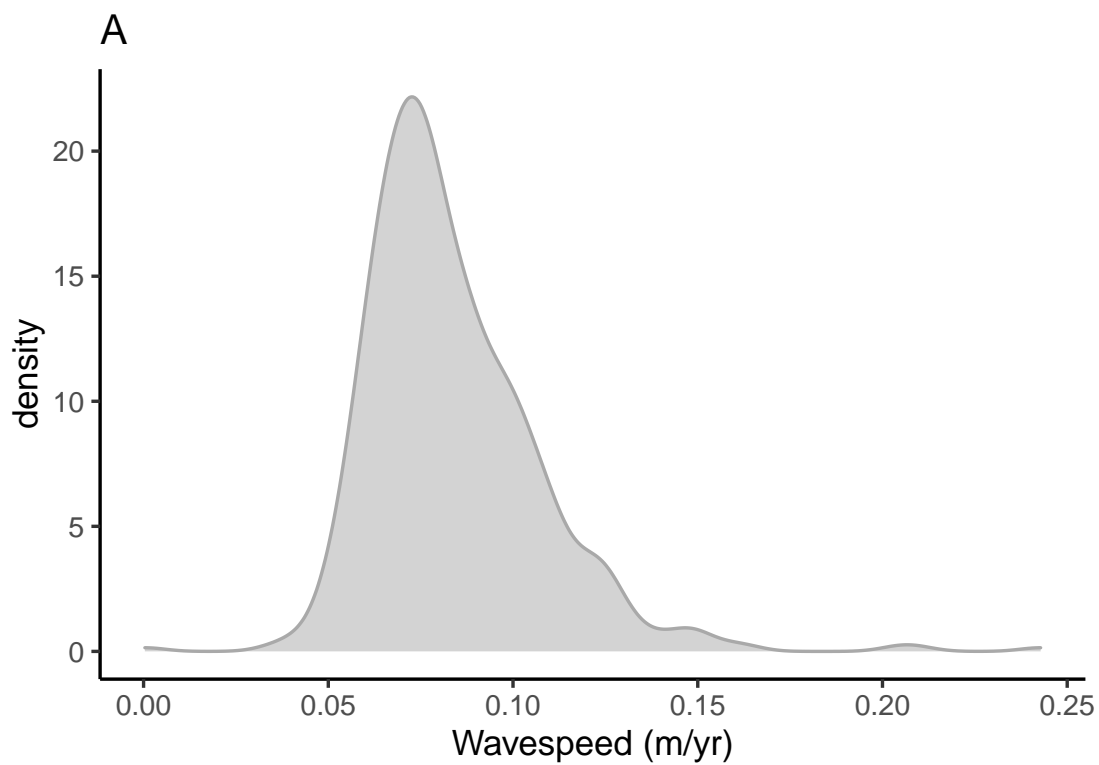


Figure 5

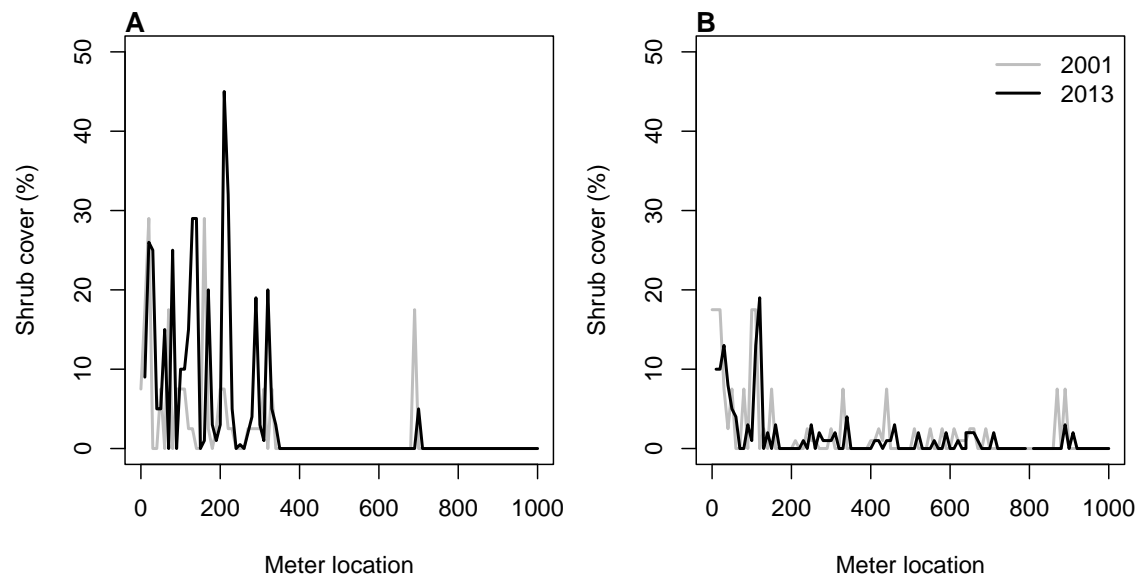


Figure 6

Appendix A: Dispersal kernel modeling

WALD dispersal kernel. In order to create the dispersal kernel, we first take the wind speeds at measurement height z_m and correct them to find wind speed U for any height H by using the logarithmic wind profile

$$U = \frac{1}{H} \int_{d+z_0}^H \frac{u^*}{K} \log \left(\frac{z-d}{z_0} \right) dz \quad (\text{A1})$$

given in Bullock et al. (2012) equation 6, with the notation slightly modified. Here, z is the height above the ground, K is the von Karman constant, and u^* is the friction velocity. The zero-plane displacement d and roughness length z_0 are surface roughness parameters that, for a grass canopy height h above the ground, are approximated by $d \approx 0.7h$ and $z_0 \approx 0.1h$. These estimates are from Raupach (1994) for a canopy area index $\Lambda = 1$ in which the sum of grass canopy elements is equal to the unit area being measured. A 0.15 m grass height at our study site gives $d = 0.105$ and $z_0 = 0.015$, which are suitable approximations for grassland (Wiernga, 1993). Calculations of u^* were done using equation A2 from Skarpaas and Shea (2007), in which

$$u^* = KU_m \left[\log \left(\frac{z_m - d}{z_0} \right) \right]^{-1} \quad (\text{A2})$$

and U_m is the mean wind velocity at the measurement height z_m . Values for the turbulent flow parameter σ were then calculated using the estimate made by Skarpaas and Shea (2007) in their equation A4, where

$$\sigma = 2A_w^2 \sqrt{\frac{K(z-d)u^*}{C_0 U}} \quad (\text{A3})$$

and C_0 is the Kolmogorov constant. A_w is a constant that relates vertical turbulence

to friction velocity and is approximately equal to 1.3 under the assumptions of above-canopy flow made by Skarpaas and Shea (2007), based off calculations from Hsieh and Katul (1997). We used maximum plant height H as a measure of z .

The values from the previous three equations give us the necessary information to calculate μ' and λ' , thus allowing us to create the WALD distribution $p(r)$. However, the base WALD model does not take into account variation in wind speeds or seed terminal velocities, which limits its applicability in systems where such variation is present. In order to account for this variation, we integrate the WALD model over distributions of these two variables using the same method as Skarpaas and Shea (2007). Additionally, the WALD model assumes seed release from a single point source, which is not realistic for creosotebush; because seeds are released across the entire height of the shrub rather than from a point source, we integrated $p(r)$ across the uniform distribution from the grass canopy height to the shrub height. Thus, under the assumptions that the height at which a seed is located does not affect its probability of being released and that seeds are evenly distributed throughout the shrub, this gives the dispersal kernel $K(r)$, where

$$K(r) = \iiint p(F)p(U)p(z)p(r) dF dU dz \quad (\text{A4})$$

and $p(F)$ and $p(U)$ are the PDFs of the terminal velocity F and wind speed U , respectively, and $p(z)$ is the uniform distribution from h to H .

Dispersal data collection. The distribution $p(F)$ in the integral above was constructed using experimentally determined seed terminal velocities. These velocities were estimated using laboratory-based seed release experiments with a high-speed camera and motion tracking software to determine position as a function of time. We then used the Levenberg-Marquardt algorithm to solve a quadratic-drag equation of motion for

965 *F.* Before seeds were released, they were dried, dyed with yellow fluorescent powder,
966 and then put against a black background to improve visibility and make tracking easier.
967 While the powder added mass to the seeds, this added mass only yielded an approx-
968 imately 2.5% increase, likely having little effect on terminal velocities. Measurements
969 were conducted for 48 seeds that were randomly chosen from a seed pool derived from
970 different plants, and then an empirical PDF of terminal velocities was constructed using
971 the data. Constructing $p(U)$ involved creating an empirical PDF of hourly wind speeds
972 using data from Sevilleta LTER meteorological station 49, the station closest to our tran-
973 sects. We used wind speed data collected hourly from 2015 to 2019 (Moore and Hall,
974 2022).

Appendix B: Additional results

Pr(Survival)	df	dAIC
~size + transplant + size:transplant + (1 transect)	11.50	1.72
~size + transplant + density + size:transplant + density:transplant + (1 transect)	13.19	0.19
~size + transplant + density + size:transplant + density:transplant + size:density + size:transplant:density + (1 transect)	14.22	0.00

Table B1: AIC model selection for survival probability.

mean(size)	sd(size)	df	dAIC
~size + (1 transect)	~1	3.00	1024.88
~size + density + (1 transect)	~1	8.50	977.23
~size + density + size:density + (1 transect)	~1	10.47	975.17
~size + (1 transect)	~size	9.65	146.23
~size + density + (1 transect)	~size	16.24	19.45
~size + density + size:density + (1 transect)	~size	18.55	19.62
~size + (1 transect)	~size + density	10.40	115.52
~size + density + (1 transect)	~size + density	18.97	0.08
~size + density + size:density + (1 transect)	~size + density	21.33	0.00

Table B2: AIC model selection for mean and variance of future size

Pr(Flowering)	df	dAIC
~size + (1 transect)	5.78	0.63
~size + density + (1 transect)	6.80	2.32
~size + density + size:density + (1 transect)	7.24	0.00

Table B3: AIC model selection for flowering probability.

No. fruits	df	dAIC
$\sim \text{size} + (1 \text{transect})$	14.25	71.99
$\sim \text{size} + \text{density} + (1 \text{transect})$	5.52	0.00
$\sim \text{size} + \text{density} + \text{size}:\text{density} + (1 \text{transect})$	6.23	0.37

Table B4: AIC model selection for fruit number.

Pr(Recruitment)	df	dAIC
$\sim (1 \text{transect})$	6.57	0.00
$\sim \text{density} + (1 \text{transect})$	7.39	0.93

Table B5: AIC model selection for recruitment probability.

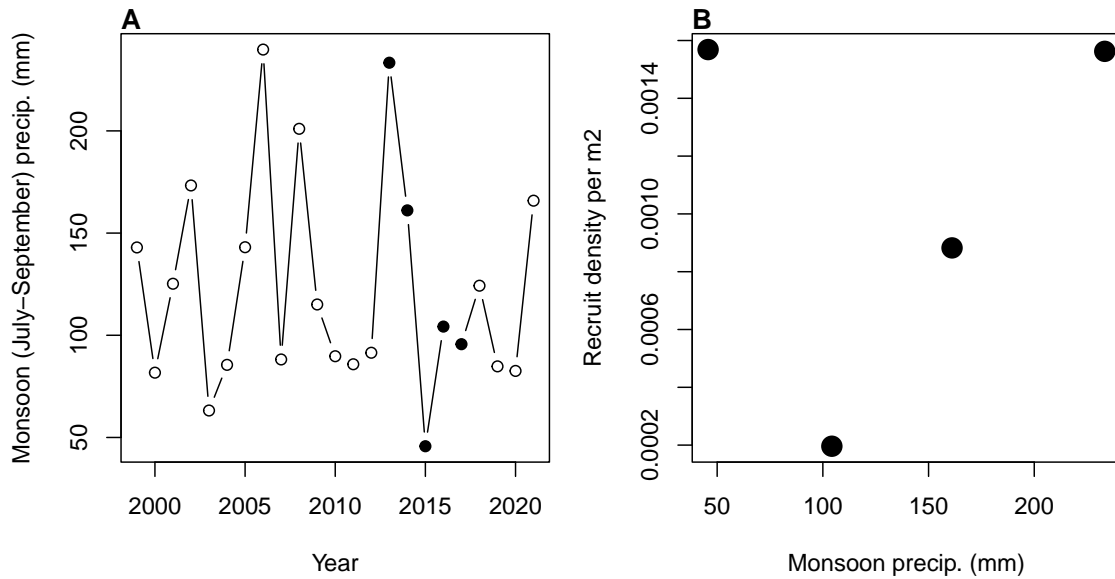


Figure B1: A, Time series of annual monsoon precipitation (filled circles are the years in which this study was conducted). B, Relationship between density of creosotebush recruits observed on our transects in May-June and monsoon precipitation in the preceding July-September.

mean(size)	sd(size)	df	dAIC
~(1 transect)	~1	2.00	2.90
~density+(1 transect)	~1	4.42	0.00
~(1 transect)	~density	3.00	4.74
~density+(1 transect)	~density	5.56	1.21

Table B6: AIC model selection for mean and variance of recruit size.

Appendix C: Additional transplant analysis

We censused transplant survival twice following July 2015 planting, in fall 2015 and spring 2016. Here, we analyze the two survival intervals separately, including grass and shrub cover at the local (1m x 1m) scale as explanatory variables in addition to the weighted density of the 5-m transect window as presented in the main text.

For both fall and spring survival censuses, we fit eight candidate models that included all combinations of window weighted density, local shrub cover (proportion of plot area covered by creosotebush), and local grass cover (proportion of plot area covered by any grass species) as smooth terms in a generalized additive model. We used a binomial response distribution where “successes” were the number of survivors per plot and “trials” were the number of seedlings planted for fall survival (always four per plot) and the number of fall survivors for spring survival. All models included a random effect of transect. We used AIC-based model selection to quantify support for competing models.

Results. The majority of mortality occurred within the first census interval (53 fall survivors out of 576 transplants), resulting in a much smaller data set for the second census interval (20 spring survivors out of 53 fall survivors).

For fall survival, the top model (Model 7) included effects of creosotebush weighted density at the 5-m window scale and local grass cover (Table C1). Fall survival was low overall but greatest in zero-density windows and there was a weak negative effect of

995 local grass cover (Figure C1). Three additional models (2, 5 and 8) were within 2 AIC
 996 units of the top model (Table C1). Despite the model uncertainty, these top four models
 997 included shrub weighted density and comprised 87% of AIC weight, providing strong
 998 support for negative effects of shrub density at the scale of 5-m windows, consistent with
 999 the full analysis (transplant experiment + observational census) presented in the main
 1000 text.

1001 Spring survival was dominated by high model uncertainty, and the most complex
 1002 model (8) did not converge due to inadequate data. The top-ranked model was Model 6,
 1003 which included effects of local shrub and grass cover. However, the null model (1) was
 1004 nearly tied with the top model, and six of seven models were within 2 AIC units. Given
 1005 the relatively small data set, a conservative interpretation is that there is not sufficient
 1006 evidence to reject the null hypothesis of a constant fall-to-spring survival rate that was
 1007 unrelated to shrub or grass density.

Pr(Survival)	df	dAIC
(1 transect)	8.93	11.98
window density + (1 transect)	9.97	0.49
shrubs cover + (1 transect)	10.82	3.51
grass cover + (1 transect)	11.02	6.65
window density + shrubs cover + (1 transect)	12.11	1.04
grass cover + shrubs cover + (1 transect)	12.29	3.29
window density + grass cover + (1 transect)	11.44	0.00
window density + shrubs cover + grass cover + (1 transect)	12.39	1.80

Table C1: AIC model selection for July-October transplant survival probability.

Pr(Survival)	df	dAIC
(1 transect)	1.00	0.07
window density + (1 transect)	2.00	1.93
shrub cover + (1 transect)	2.00	1.22
grass cover + (1 transect)	2.03	0.69
window density + shrub cover + (1 transect)	3.00	1.85
grass cover + shrub cover + (1 transect)	3.37	0.00
window density + grass cover + (1 transect)	3.23	2.19

Table C2: AIC model selection for October-June transplant survival probability.

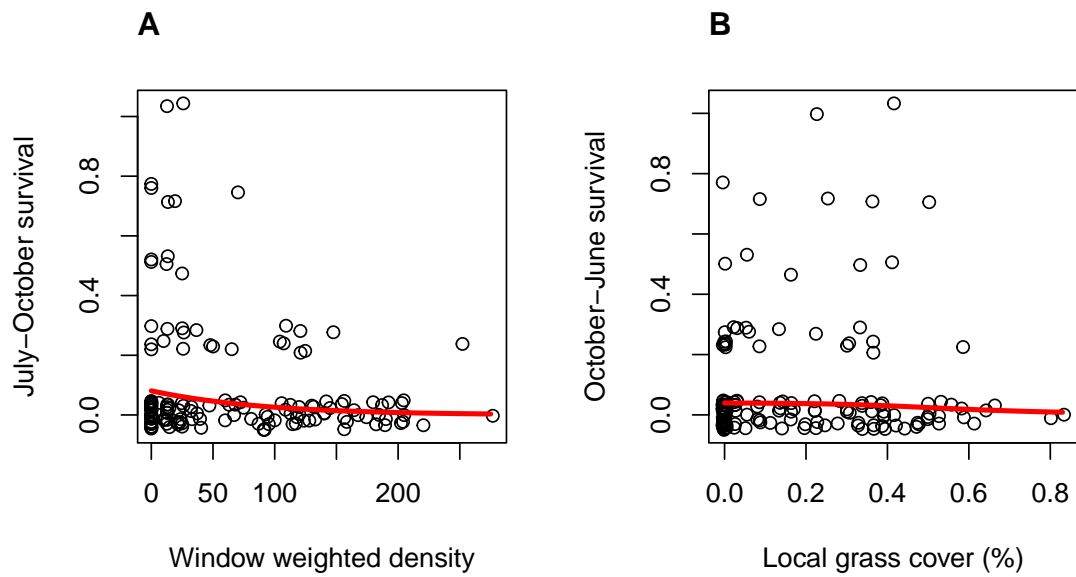


Figure C1